An Efficient and Fast, Noninvasive, Auto-Fluorescence Detection Method for Early-Stage Oral Cancer

Ning Wang, *Member, IEEE*, Yuan Liu, and Hongwen Li

***Abstract*— This article proposes an efficient and fast auto-fluorescence method for early-stage oral cancer detection. Using mechanical composition analysis and 3-D modeling, the simple automatic equipment prototype with noninvasive detection and real-time observation is constructed. Herpes simplex, sublingual gland cysts, and biological enzyme solutions [flavin adenine dinucleotide (FAD) and nicotinamide adenine dinucleotide (NADH)] at different concentrations are detected using a 560-nm filter with a bandwidth of 30 nm, and ultraviolet LED (UV-LED) light sources at 3 and 5 W with wavelengths of 375, 395, 405, 410, and 420 nm, respectively. Also, the applicability of the detection conditions for several regions of the oral cavity is demonstrated in detail. Experimental results show that the specificity of 0.95 by selecting UV-LED with specific wavelength and observing the characteristics of lesions. The proposed detection method will be helpful in screening oral cancer and auto-detection of precancerous lesions.**

***Index Terms*— Auto-fluorescence, flavin adenine dinucleotide (FAD), nicotinamide adenine dinucleotide (NADH), oral cancer detection, ultraviolet LED (UV-LED).**

I. Introduction

ORAL cancer is a malignant tumor that occurs in the buccal mucosa, upper/lower gums, hard palate, tongue, and floor of the mouth. It includes the lip/oral cavity carcinoma, salivary glands, oropharynx, nasopharynx, and hypopharynx. The main symptoms include having long-term unhealed or repeated ulcers on the oral mucosa, feeling pain, numbness, difficulty swallowing, sudden loosening of multiple teeth, and having lumps or nodules [1]. The reported risk factors for oral cancer are mainly tobacco [2]–[5], alcohols [3]–[6], and betel quid [5], [7], [8]. Some studies also indicate there is a risk of oral cancer due to dietary habit [4], [5] and human papillomavirus [3], [9], [10]. At present, globally, the diagnosis of oral cancer in patients is delayed. This is because of insufficient medical resources and the lack of qualified medical personnel and diagnostic tools [11], [12]. For example, when most patients feel discomfort in the oral cavity, they will contact the family doctor or dental clinic. In many cases, these facilities may not have resources for oral pathological biopsy. This means that only a preliminary oral examination can be done, even though the diagnosis sensitivity highly depends on the doctor's experience. According to a study by Lingen *et al.* [13], by the time more than 60% of patients were diagnosed, the tumor had progressed to the third and fourth stages. Additionally, the lesion area had reached a size visible to the naked eye [13]. It is estimated that about 80% of patients can live for five years if oral cancer can be detected and located at an early stage [14]–[16]. Therefore, it is necessary to study and develop effective and quick detection methods for early-stage oral cancer and oral precancerous lesion [17]. Meanwhile, cost and portability should also be considered for the detection methods if they are to be promoted and used globally.

At present, oral cancer is the sixth most common cancer, with a poor prognosis and a five-year survival rate of about 30%–60% [18]–[20]. Early diagnosis and early treatment are the keys to improving patients' survival rate and quality of life [14]. However, the tumor may have infiltrated and metastasized when patients present with clinical symptoms such as pain, bleeding, ulcers, or masses that affect language or swallowing [13]. Therefore, before patients present with clinical symptoms, the screening of high-risk groups for export cavity cancer and early diagnosis should be the goal for all clinicians. In addition to routine examination of oral lesions, *in vivo* staining, spectral analysis, and brush biopsy of oral tissue are expected to enhance early-stage oral cancer diagnosis [13], [21]. However, the relative accuracy and timeliness of early-stage oral cancer detection methods are not ideal [13], [22]. Due to no significant border distinctness, an accuracy of only 18.2% is obtained in ViziLite examination method for 55 lesion patients, resulting in little benefit to lesion detection (as a screening device) or diagnosis (as a case-finding device) [13]. In addition, the repeated intra-oral examination with standard operatory lighting in the ViziLite system spends a lot of time. Petruzzi *et al.* [22] achieved a specificity of 0.577 using autofluorescence ancillary examination method with histopathological findings in lesions. However, it is not specific enough to distinguish noncancerous lesions from true cancerous lesions in the general population [22].

Table I shows a variety of fluorescence screening methods for oral cancer. Based on multispectral lifetime imaging technology, Jo *et al.* [23] used pulsed laser as excitation

Manuscript received 9 May 2022; accepted 24 June 2022. Date of publication 22 July 2022; date of current version 29 July 2022. This work was supported by the Natural Science Foundation of Shanghai through grant 21ZR1446300, and the National Key Research and Development Program of China through grant 2018YFA0701800. The Associate Editor coordinating the review process was Dr. Rosenda Valdes Arencibia. *(Corresponding author: Hongwen Li.)*

The authors are with the Shanghai Key Laboratory of Modern Optical System, Engineering Research Center of Optical Instrument and System, Ministry of Education, University of Shanghai for Science and Technology, Shanghai 200093, China (e-mail: 13262617365@163.com).

Digital Object Identifier 10.1109/TIM.2022.3191655

TABLE I
COMPARISON TABLE OF FLUORESCENCE DETECTION METHODS

	Jo et al. [23]	Shaiju et al. [24]	Huang et al. [25]	Lalla et al. [26]	This Work
Method	Multispectral Fluorescence Lifetime Imaging	Spectra Analysis	Auto-fluorescence Detection	Auto-fluorescence Detection	Auto-fluorescence Detection
Output Mode	Fluorescence Lifetime Image	Fluorescence Spectra	Fluorescence Image	Fluorescence Image	Fluorescence Image
Excitation Light Source	Pulsed Laser (355 nm)	Xenon Lamp	UV-LED (400-460 nm)	LED (white light, 405 nm and 545 nm)	UV-LED (375, 395, 405, 410, and 420 nm)
Main Configuration	Pulsed laser + Rigid Endoscope + Fiber + Photomultiplier Tube etc.	Xenon Lamp + Fiber + Spectrofluorometer	VELscope Device	Identafi Device	UV-LED + Fiber + Dichroic Mirror + Emission Filter
Specificity	0.87	0.95	0.923	0.85	0.95

source and collected fluorescence lifetime images. The detection results showed a specificity of 0.87. However, although the fluorescence lifetime images can be used to screen oral cancer, compared with autofluorescence technology, the use of photomultiplier tubes to collect fluorescence signals is slightly inadequate in the visual observation of the lesions. Shaiju *et al.* [24] used Xenon lamp as excitation light source, collected and analyzed spectra with spectrometer, and achieved a specificity of 0.95. While the output mode of the results is fluorescence spectra, which cannot show the distribution of the lesion in the wide field of vision like autofluorescence technology, or realize the naked eye observation of the lesion. Huang *et al.* [25] used VELscope (White Rock), UV-LED of the wavelength between 400 and 460 nm as the excitation light source, and applied quadratic discriminant analysis to analyze the detected images. A specificity of 0.923 has been obtained. In addition, Lalla *et al.* [26] performed autofluorescence detection using Identafi (DentalEZ) and achieved a specificity of 0.85. However, Vigneswaran's study pointed out that fluorescence loss would also occur in the lesions of some benign inflammations, which leads to false positives and results in unnecessary panic or biopsy operations for patients [27].

Therefore, to improve the application of automated fluorescence detection technology in oral cancer screening and precancerous lesion detection, this article developed an autofluorescence detection model, and realizes the real-time visual examination with naked eyes. Meanwhile, according to the detection results, the strategy of using the different wavelengths UV-LED and observing the characteristics of images, which can reduce the influence of two kinds of benign causing lesions of false positive effect has been discussed, and a specificity of 0.95 has been achieved. The proposed detection equipment should have a low cost, simple structure, and efficient inspection results, and this is conducive to promoting automated fluorescence technology in the field of insufficient medical resources.

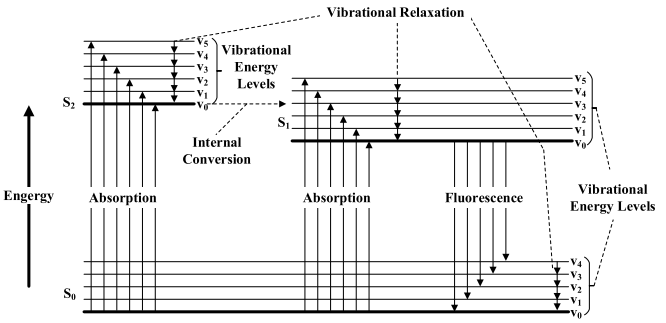

Fig. 1. Jablonski diagram. (In this work, only the singlet state of electrons has been considered, denoted as S. For the excitation to the triplet state, phosphorescence will be produced in a relatively similar way, which is not discussed in this work.)

The rest of this article is organized as follows: Section II systematically introduces the theoretical basis of autofluorescence. Section III introduces the prototype design of auto-fluorescence detection system in detail. In Section IV, auto-fluorescence detection is carried out and the simulation results are compared. Finally, Section VI summarizes the conclusions of the test results.

II. THEORETICAL BASIS

A. Auto-Fluorescence

Auto-fluorescence refers the natural fluorescence emitted by biological structures after absorbing photons [28]. The generation of fluorescence is shown in Fig. 1 [29], [30]. The absorption of light takes molecules from the ground state S_0 to excited electronic states S_1 and S_2. The excited molecules give up energy and step down to the lowest vibrational energy level $S_1(\upsilon_0)$ by means of nonradiative transitions including vibrational relaxation and internal conversion [31]. Following Kasha's rules, energy will be further released in the form of photons, which is fluorescence, during the transition from the lowest energy level of $S_1(\upsilon_0)$ to the different energy levels of S_0 [30], [32].

B. Fluorophores in the Oral Cavity

The auto-fluorescence detection object of oral cancer is a variety of fluorophores in oral tissues, including coenzyme, collagen, cross-linking, and porphyrin. The coenzyme is an organic compound that binds to enzyme proteins in the human body and performs catalytic actions. Flavin adenine dinucleotide (FAD) and nicotinamide adenine dinucleotide (NADH) are two kinds of enzymes that are essential parts of the respiratory chain of the human body. Their concentrations change with the canceration of cells.

FAD is a coenzyme of a variety of oxidoreductases (dehydrogenases) in the human body. The left part of Fig. 2 shows that the N atom on the isoalloxazine ring in the FAD structure can undergo reversible dehydrogenation and hydrogenation reactions. It is mainly responsible for transferring the electrons

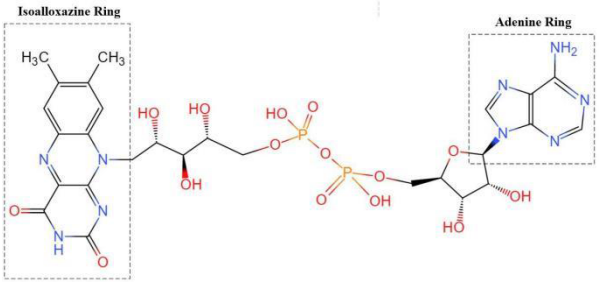

Fig. 2. Schematic of the structure of FAD, $C_{27}H_{33}N_9O_{15}P_2$.

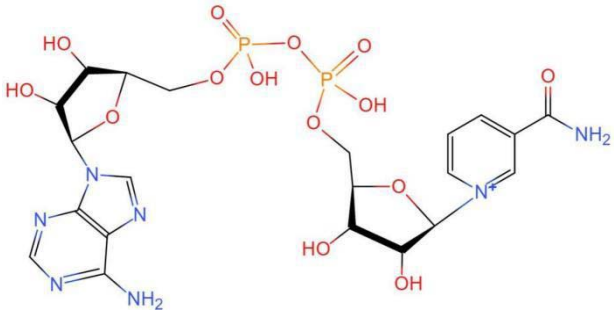

Fig. 3. Schematic of the structure of NADH, $C_{21}H_{27}N_7O_{14}P_2$.

obtained from the oxidation of the substrate by the dehydrogenase with FAD as the coenzyme and is involved in transferring hydrogen atoms.

Meanwhile, according to work in [33], the fluorescence efficiency of FAD might be related to the position between the isoalloxazine ring and the adenine ring. Fig. 2 shows the structure of FAD, including an isoalloxazine ring and an adenine ring. When FAD is in an excited state, the structure will change from the open state to the stacking of the isoalloxazine ring and the adenine ring, and finally, the fluorescence will be quenched entirely [34].

Similar to FAD, NADH (see Fig. 3) also produces fluorescence when excited by an external light source and is the major fluorophore in oral tissues. NADH is widely present in organisms, mainly involved in the metabolism of substances and energy.

C. Auto-Fluorescence Detection

The principle of auto-fluorescence detection used in this work applies an ultraviolet light source to the oral cavity. The fluorophores described in Section II-B emit auto-fluorescence because of the excitation and then detect the fluorescence of the oral tissue.

When oral tissue undergoes cancerous transformation or precancerous lesion formation, cancer cells divide out of control, and the redox activity inside the cells increases. As the main components of the respiratory chains, concentrations of FAD and NADH will rise accordingly. At the same time, the structural fibers of collagen and matrix are destroyed. This results in increased fluorescence produced by coenzymes and decreased fluorescence produced by collagen. But in the dominant position, the auto-fluorescence of the whole lesion area will be reduced, and there will be a phenomenon of lack of fluorescence [35]. In addition, the increase in hemoglobin absorption, epithelial scattering, and the thickness of the epithelium are some reasons for the lack of fluorescence [36].

In cases such as oral leukoplakia, the thicker keratinized layer in the upper jaw and gums of the patient can also cause the phenomenon of lack of fluorescence. In addition, for some chronic inflammatory diseases, lymphocytes will be activated by antigen stimulation, and a large number of them will accumulate in the focus area. The structural fibers of the matrix will be destroyed because of the expression of matrix-degrading protease, which will also cause the phenomenon of lack of fluorescence [35].

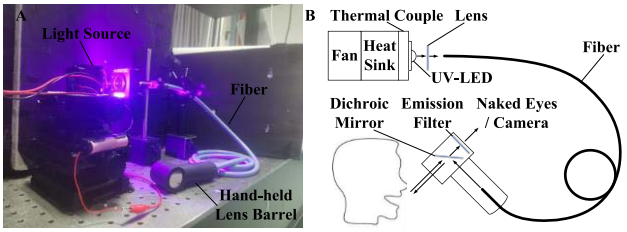

Fig. 4. (a) Fabricated model of the proposed design. (b) Schematic of auto-fluorescence detection equipment.

III. Prototype Design

In this work, application scenarios and usage methods have been considered in designing auto-fluorescence detection equipment. First, it is necessary to clarify that the detection equipment should be used as an auxiliary means of a routine oral examination. Considering the primary location for most patients with oral discomfort, the main application scenario should be small and medium-sized dental clinics or family doctors in remote areas. This means that the detection equipment needs to have a simplified structure with convenient mobility, low equipment cost, and low maintenance cost. Therefore, a prototype of an auto-fluorescence oral cavity detection device was built combined with the principle of auto-fluorescence detection (see Fig. 4).

Fig. 4(a) shows that the detection equipment contains three main modules: light source, light guide fiber, and hand-held lens barrel. As shown in Fig. 4(b), the working principle is that light near the ultraviolet band emitted by the LED cooled by the thermocouple is collected by the lens and then transmitted to the hand-held observation lens barrel by the optical fiber, and the dichroic mirror reflects the UV light to the oral tissue. The dichroic mirror will block the UV light reflected by the oral tissue, and the generated auto-fluorescence will pass through the dichroic mirror and emission filter.

Many documents in Section II-C indicate that the specific wavelength band that is most suitable for the excitation light of the oral tissue has not yet been identified, but most of the cases are concentrated in the vicinity of the ultraviolet wavelength band. Therefore, to study the influence of different wavelength

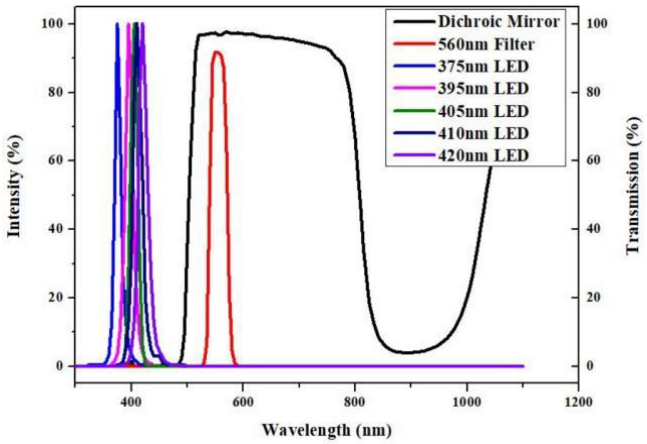

Fig. 5. Transmittance of the dichroic mirror and filter with the spectrum of UV-LED.

light sources on the imaging of oral auto-fluorescence detection, the light source part of the equipment uses multiple different wavelengths (375, 395, 405, 410, and 420 nm) and different power ultraviolet LED (UV-LEDs), which are shown in Fig. 5. These LEDs are all welded to the aluminum substrate and can be placed in the position shown in Fig. 4. The power supply for each LED is a 3.7-V (18 650) lithium battery.

The collection and observation of fluorescence are also essential in auto-fluorescence detection. In this equipment, the spectrum of the excitation light source used is all around the ultraviolet wavelength band. An emission bandpass filter with maximum transmittance at 560 nm (30 nm bandwidth) is used to collect fluorescence (see Fig. 4). Thus, the dichroic mirror (45° incidence) can reflect the excitation light and transmit the fluorescence (see Fig. 5). Moreover, the dichroic mirror can also make the direction of excitation light irradiation to be in the same horizontal direction as the direction of fluorescence observation. In addition, a cavity made of nylon was fabricated as the tube (using 3-D printing technology) to achieve the characteristics of lightness, drop resistance, and ease of operation.

Meanwhile, considering that the heat generated by UV-LED, a cooling system combined with the thermocouple, heat sink, and fan (see Fig. 4) is used to control the temperature of the LED. The essence of thermocouple work is semiconductor thermoelectric cooling, and this principle mainly applies to the Peltier effect. This effect occurs when the current flows through the extrinsic semiconductor in one direction, one end of the semiconductor will absorb heat, and the other end will emit heat. The endothermic and exothermic phenomena of the ends of n-type semiconductors and p-type semiconductors are just opposite. When the n-type and the p-type are combined (see Fig. 6), a thermocouple is formed, and the cooling effect can be achieved by stacking multiple thermocouples. The advantage of this heat dissipation method is that it can be actively cooled and has a long service life. It can also be combined with other cooling methods to achieve a further cooling effect through a heat sink.

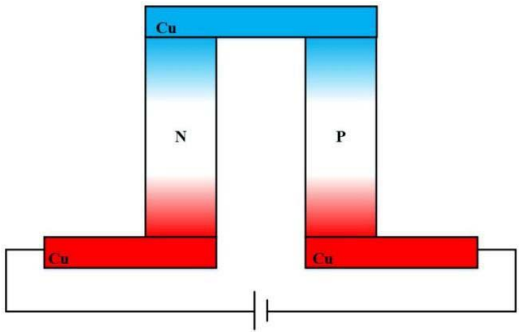

Fig. 6. Schematic of thermocouple structure.

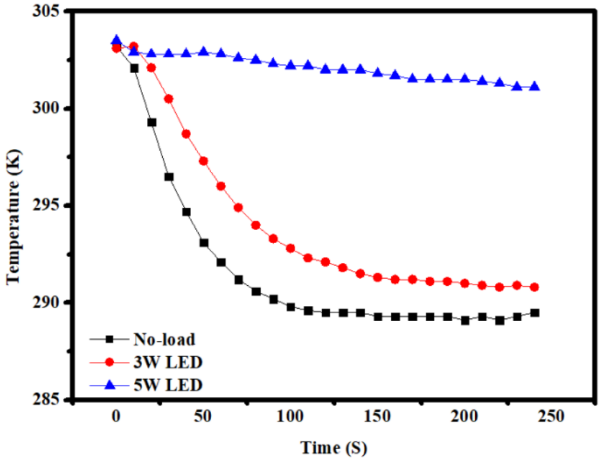

Fig. 7. Cooling capacity of the thermocouple cooling part over time.

Fig. 4 shows that the UV-LED is placed on the thermocouple in this work so that the aluminum substrate directly contacts the cooling surface. A heat sink is placed on the hot end of the thermocouple to conduct heat by increasing the contact area with the air and then using a dc fan to accelerate air circulation and heat dissipation. In addition, to consider the portability of the testing equipment, the thermocouple and the dc fan are powered by a 5.1-V lithium battery. The cooling efficiency of the cooling part is shown in Fig. 7. When the refrigeration part is started at room temperature (0 s), the thermocouple surface temperature drops sharply at the beginning. Over time, the equilibrium point is reached about 120 s, at which time the temperature drops by about 19 K in total. It shows that the refrigeration part combined with semiconductor cooling and air cooling achieves a fast and better cooling effect.

IV. Auto-Fluorescence Detection and Results

In this article, in order to verify the effectiveness and applicability of the prototype of auto-fluorescence detection equipment and study the interference of herpes simplex and sublingual gland cyst with the detection, lesions of two inflammations, FAD, and NADH solution has been detected within the proposed model.

Since the excitation light source is UV-LED, all volunteers must wear laser protective glasses with a protection

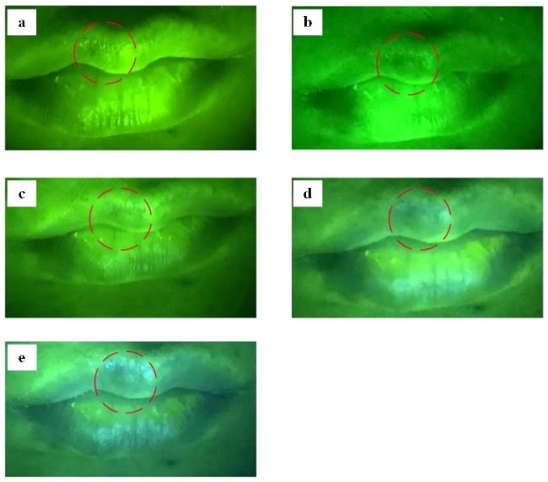

Fig. 8. Auto-fluorescence detection image of a patient with herpes simplex. (a)–(e) Excited by 3-W LEDs at 375, 395, 405, 410, and 420 nm, respectively.

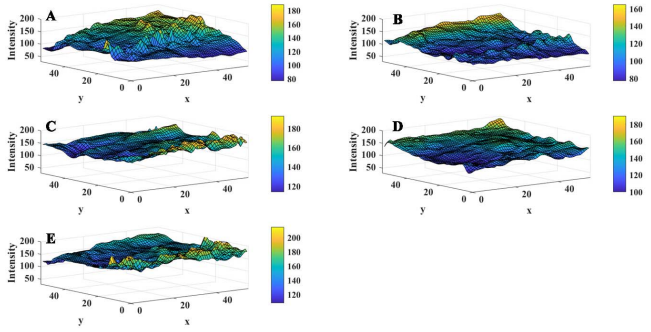

Fig. 9. Color maps of intensity for auto-fluorescence detection image of a patient with herpes simplex. (a)–(e) Excited by 3-W LEDs at 375, 395, 405, 410, and 420 nm, respectively.

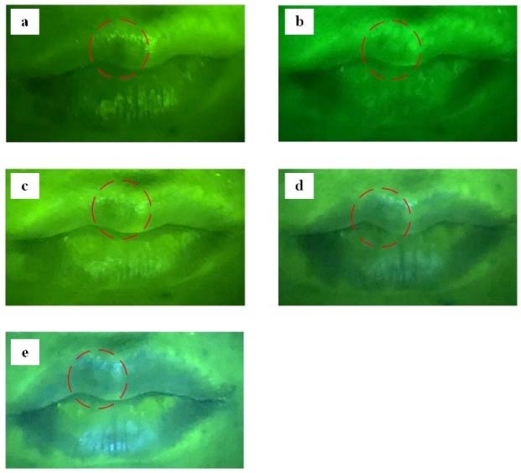

Fig. 10. Auto-fluorescence detection image of a patient with herpes simplex. (a)–(e) Excited by 5-W LEDs at 375, 395, 405, 410, and 420 nm, respectively.

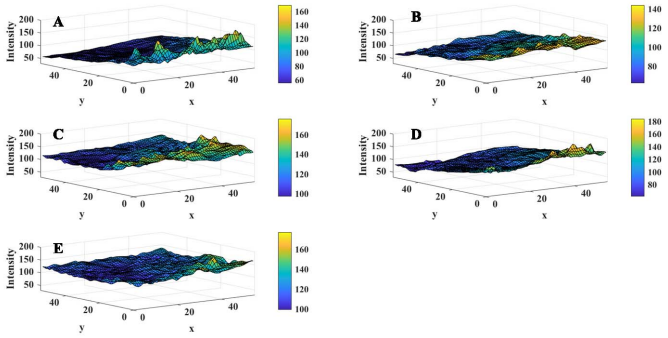

Fig. 11. Color maps of intensity for auto-fluorescence detection image of a patient with herpes simplex. (a)–(e) Excited by 5-W LEDs at 375, 395, 405, 410, and 420 nm, respectively.

wavelength of 190–470 nm during the inspection experiment to protect their eyes. In addition, experiments were carried out in a room without other light sources to simulate the oral inspection environment and exclude external influences. Before running the oral auto-fluorescence examination, all volunteers must also use 0.9% normal saline to rinse their mouths for 2 min. Auto-fluorescence photos are captured with a mobile phone camera.

A. Herpes Simplex Detection

Herpes simplex is caused by the herpes simplex virus, which can heal on its own. However, after the initial infection, it will change to the latent state, and it will recur when the patient receives external stimuli. The main clinical manifestations of recurrent herpes simplex are feeling pain and burning in the skin or mucous membranes, followed by the formation of blisters in the lesion area, prone to erosion, exudation, and crusting.

Using the proposed auto-fluorescence detection method, the experiment with different LED wavelengths and power magnitudes is carried out (see Figs. 8–11). The targeted case is a patient with herpes simplex (male, 25 years old, no history of smoking) and has been clinically diagnosed. The patient was in the onset period when he was examined, and the main observation area was blisters on the lips. It can be seen from Figs. 8 and 9 that the fluorescent images of the blisters marked by the red circle are different under the excitation of LEDs of different wavelengths. Through comparison, it can be found that when excited by a light source with a wavelength of 395 nm, the inflammatory lesion area has a relatively noticeable fluorescence contrast effect. The central part has a lower fluorescence intensity, and the edge of the lesion can be observed very clearly, which causes a clear contrast with the same area on the other side of the upper lip. This shows that when the detection device uses a 395-nm light source to detect the lips, the lesion area caused by herpes simplex may cause a false positive effect on cancer detection. While, by observing the fluorescence imaging of the 405-nm wavelength LED, the change in fluorescence intensity caused by inflammation is less noticeable. This indicates that using this work mode, the equipment is not sensitive to the inflammation, and the specificity of auto-fluorescence detection can be improved.

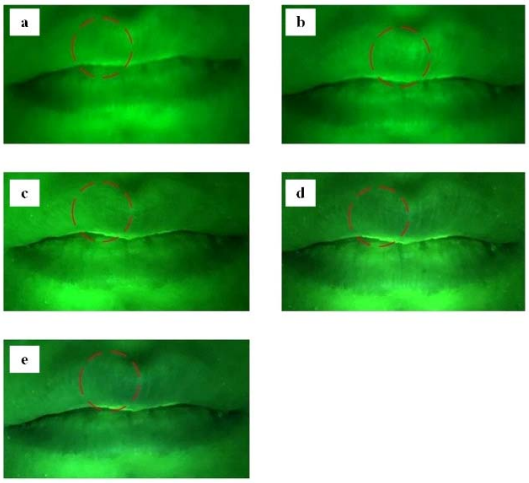

Fig. 12. Auto-fluorescence detection image of lips of healthy volunteers. (a)–(e) Excited by 3-W LEDs at 375, 395, 405, 410, and 420 nm, respectively.

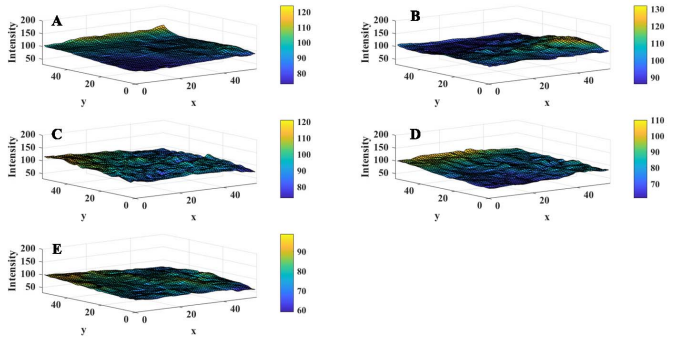

Fig. 13. Color maps of intensity for auto-fluorescence detection image of lips of healthy volunteers. (a)–(e) Excited by 3-W LEDs at 375, 395, 405, 410, and 420 nm, respectively.

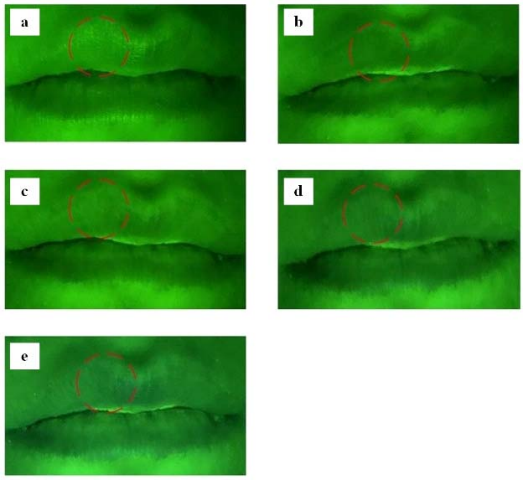

Fig. 14. Auto-fluorescence detection image of lips of healthy volunteers. (a)–(e) Excited by 5-W LEDs at 375, 395, 405, 410, and 420 nm, respectively.

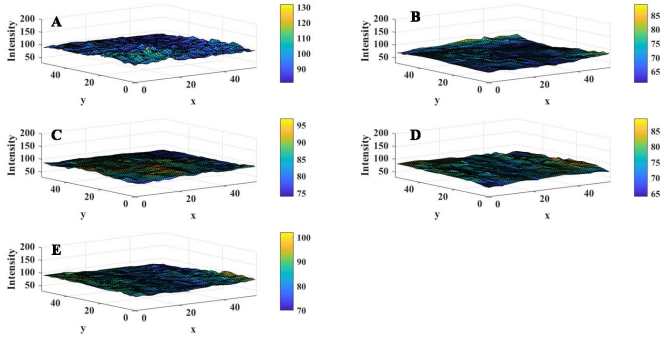

Fig. 15. Color maps of intensity for auto-fluorescence detection image of lips of healthy volunteers. (a)–(e) Excited by 5-W LEDs at 375, 395, 405, 410, and 420 nm, respectively.

Figs. 10 and 11 show the application of a 5 W LED for excitation, and the wavelength is the same as the above experiment. The findings show that after increasing the excitation light power, a clearer focus area of lesion can be observed using the LED with a wavelength of 395 nm and lower interference from inflammatory lesions under the LED with a wavelength of 405 nm. This is consistent with the 3-W LED excitation results. It also indicates that, compared with the change of light power from 3 to 5 W, the fluorescence of the herpes simplex lesions is mainly sensitive to the wavelengths of excitation light.

The examination photos of the healthy control group are shown in Figs. 12–15 (female, 23 years old, no smoking history). Here, it can be seen that the observation site marked by the red circle and the same part on the other side of the upper lip layer have relatively the same fluorescence imaging effect, where there is no edge of the lesion in this area and its surroundings (see Fig. 8). Comparing the auto-fluorescence images of Figs. 8, 10, 12, and 14, it can be found that the observed area of the normal upper lip blister does not have different intensity of fluorescence compared with the surrounding area. Therefore, we can confirm that the relatively obvious fluorescence contrast in Figs. 8, 9, 12, and 13 is caused by the lesion, which also shows a good improvement in preventing the disturbance of herpes simplex for this detection method.

B. Sublingual Gland Cyst Detection

Sublingual gland cysts are salivary gland mucinous cysts caused by damage to the glands or ducts. With the continuous penetration of mucus into the tissues, cysts will gradually form. Sublingual gland cysts will not heal on their own, and surgical methods are usually needed to remove the glands in the cyst area of the patient. The primary clinical manifestation of the simple sublingual gland cyst is that it is located under the mucosa on the bottom side of the mouth. It is translucent or light blue in the initial stage and will gradually increase with the patient's saliva secretion behavior such as eating, and its interior is wrapped with viscous liquid.

In this work, the auto-fluorescence detection of the sublingual gland cyst is also carried out using the proposed equipment. The targeted case is a patient with a sublingual gland cyst (male, 25 years old, no smoking history), which has been clinically diagnosed, while the patient has not removed the cyst by surgery. The main field of view, in this case,

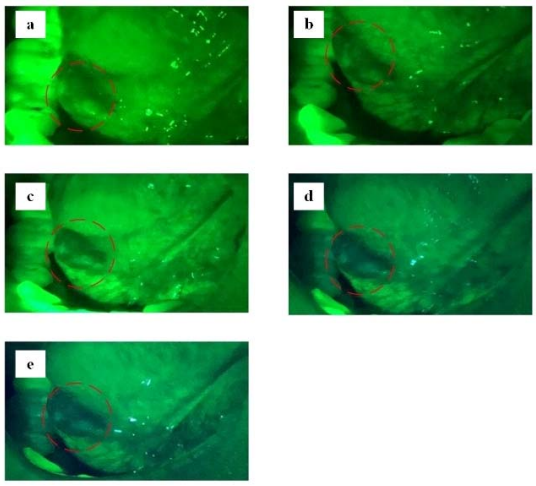

Fig. 16. Auto-fluorescence image of a patient with sublingual gland cyst. (a)–(e) Excited by 3-W LEDs at 375, 395, 405, 410, and 420 nm, respectively.

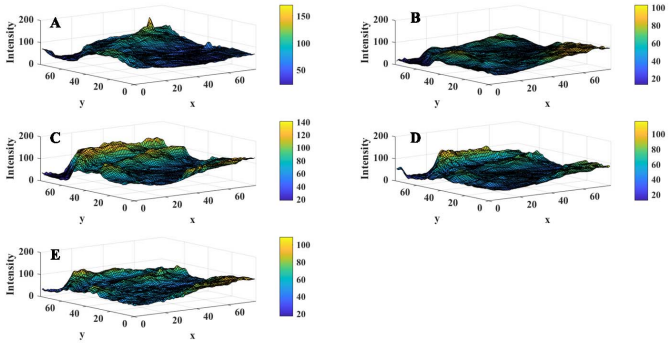

Fig. 17. Color maps of intensity for auto-fluorescence detection image of a patient with sublingual gland cyst. (a)–(e) Excited by 3-W LEDs at 375, 395, 405, 410, and 420 nm, respectively.

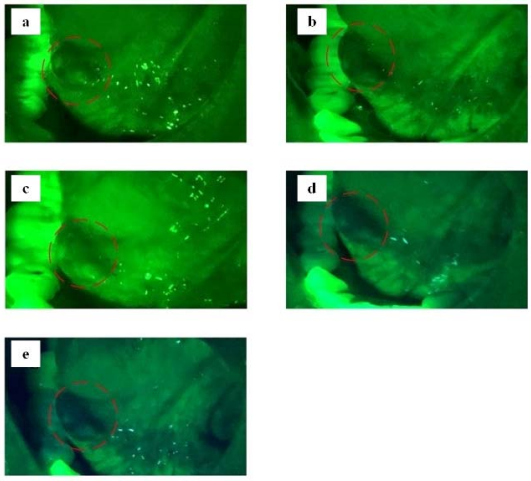

Fig. 18. Auto-fluorescence image of a patient with sublingual gland cyst. (a)–(e) Excited by 5-W LEDs at 375, 395, 405, 410, and 420 nm, respectively.

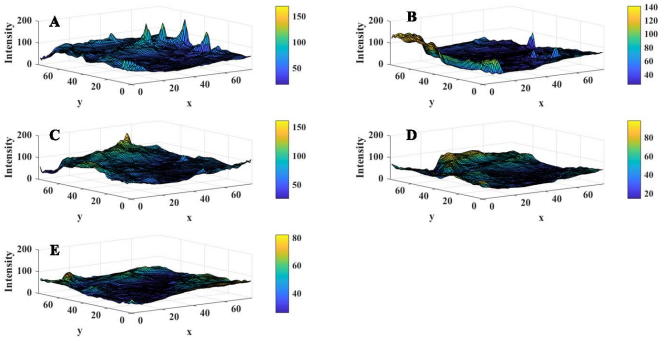

Fig. 19. Color maps of intensity for auto-fluorescence detection image of a patient with sublingual gland cyst. (a)–(e) Excited by 5-W LEDs at 375, 395, 405, 410, and 420 nm, respectively.

is the patient's cyst site, and the auto-fluorescence images and colormaps of intensity are shown in Figs. 16–19, respectively.

The auto-fluorescence images excited by the lower power LED (see Figs. 16 and 17). It can be easily seen that the lesion area of the sublingual gland cyst marked by a red circle has fluorescence loss under all excitation LEDs, and the edge of the cyst can be observed clearly. This indicates that the sublingual gland cyst is less sensitive to the change of excitation wavelength which is selected. While the areas of loss are mainly concentrated in the margin of the cyst, it can still be observed that a few fluorescent spots are at the center of the protruding top of the cyst. It is speculated that this phenomenon results from the lack of fluorophores in the mucus contained in the patient's sublingual cyst compared with the surrounding normal tissue. Therefore, although the sublingual gland cyst has a noticeable fluorescence loss effect, it can still be distinguished by its unique fluorescence image to reduce the false-positive situation when using the equipment proposed in this article.

Figs. 18 and 19 show the auto-fluorescence results of sublingual gland cyst under the excitation of LEDs with a power of 5 W. It can be seen that the cyst still has a loss of fluorescence with a noticeable edge under the excitation of LEDs with different wavelengths. There was no significant change in fluorescence intensity contrast between the cyst and normal tissue. Moreover, the fluorescence loss in the margin and the few fluorescent spots at the center of the protruding top of the cyst can still be seen (see Figs. 18 and 19). This indicates that in the mode of high excitation power of detection equipment, the sublingual gland cyst can also be distinguished by comparing fluorescence images.

The healthy control group is shown in Figs. 20–23 (female, 23 years old, no smoking history). It can be seen that the anterior part of the normal sublingual gland (the area marked by the red circle) has similar auto-fluorescence characteristics with the surrounding normal tissues. Therefore, in combination with the results observed, it can be confirmed that the loss of fluorescence shown in Figs. 20–23 is caused by the sublingual gland cyst under the excitation of UV-LED. This also proves the effectiveness of the proposed detection method in this article.

In general, comparing Figs. 9 and 11 with Figs. 13 and 15, respectively, it can be easily seen that for herpes simplex, the surface of intensity of lesions has several sunken areas than the

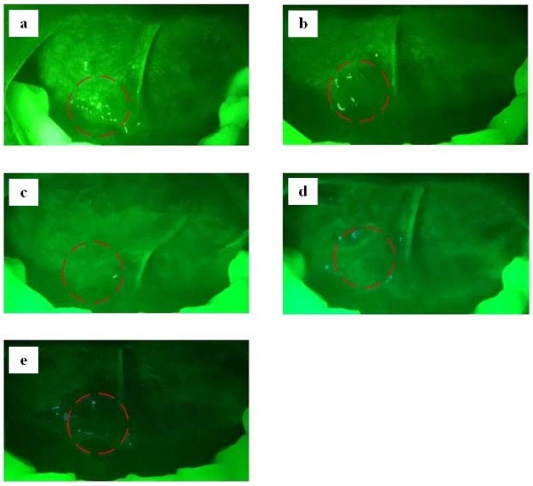

Fig. 20. Auto-fluorescence detection image of the sublingual gland of healthy volunteers. (a)–(e) Excited by 3-W LEDs at 375, 395, 405, 410, and 420 nm, respectively.

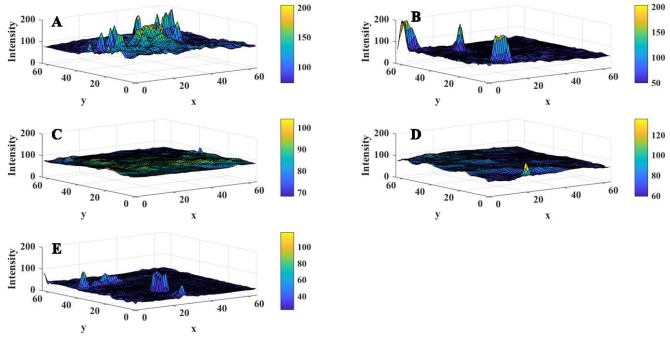

Fig. 21. Color maps of intensity for auto-fluorescence detection image of the sublingual gland of healthy volunteers. (a)–(e) Excited by 3-W LEDs at 375, 395, 405, 410, and 420 nm, respectively.

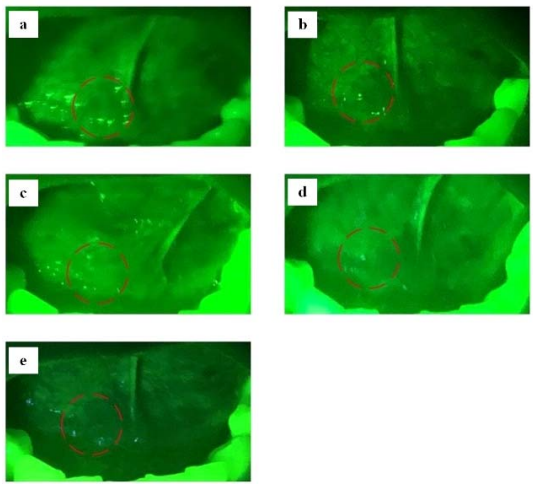

Fig. 22. Auto-fluorescence detection image of the sublingual gland of healthy volunteers. (a)–(e) Excited by 5-W LEDs at 375, 395, 405, 410, and 420 nm, respectively.

healthy control group, which is the part of fluorescence losing. The surfaces in Figs. 13 and 15 are both much smoother, which present the normal tissue. The high contrast of flatness of color

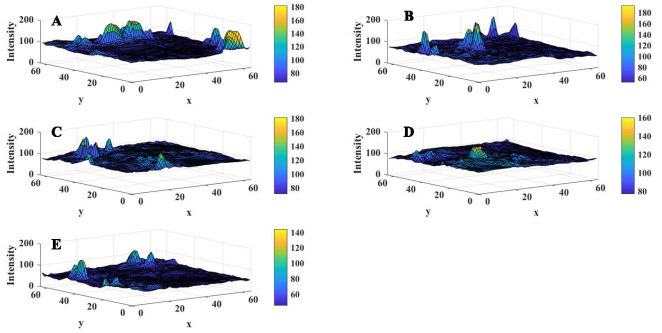

Fig. 23. Color maps of intensity for auto-fluorescence detection image of the sublingual gland of healthy volunteers. (a)–(e) Excited by 5-W LEDs at 375, 395, 405, 410, and 420 nm, respectively.

TABLE II
IMAGE HETEROGENEITY OF AUTO-FLUORESCENCE DETECTION RESULTS

Detection Group	Power of UV-LED	Wavelength of UV-LED				
		375nm	395nm	405nm	410nm	420nm
Herpes Simplex	3W	22.1	16.6	14.8	15.6	17.8
	5W	20.9	17.2	17.4	20.9	12.5
Healthy Control Group of Herpes Simplex	3W	8.2	8.5	7.2	8.3	5.6
	5W	6.4	3.4	4.1	3.5	4.3
Sublingual Gland Cysts	3W	19.8	15.8	22.5	15.9	14.6
	5W	13.1	22.7	16.8	14.1	12.1
Healthy Control Group of Sublingual Gland Cysts	3W	20.3	14.2	6.8	7.4	7.7
	5W	14.1	12.1	8.9	10.4	9.2

maps is the statistical presentation of the observing in auto-fluorescence detection images. Similarly, the high contrast of flatness also appeared in Figs. 17 and 19 with Figs. 21 and 23, which shows the same observation with auto-fluorescence detection images of sublingual gland cysts and healthy control group.

Besides, the standard deviation of intensity of image has been calculated to present the heterogeneity according to the method in [37] and [38], shown as below

$$\sigma = \sqrt{\frac{\sum (I(x, y) - \mu)^2}{n - 1}}$$

where σ, I, x, y, μ, and n are image heterogeneity, intensity of pixel, pixel counts in the x-direction, pixel counts in the y-direction, mean of intensity, and number of total pixel counts. The results are shown in Table II. And it can be easily seen, in general, the heterogeneities of herpes simplex and sublingual gland cysts are all greater than their healthy control groups, respectively. It means that the lesions of these two inflammations will cause a loss of fluorescence which might decrease the specificity of detection. But with the constructed detection model, the specificity of about 0.95 could be achieved using the proposed strategy, which is

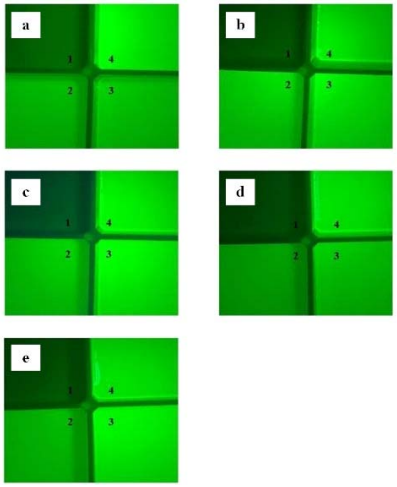

Fig. 24. Auto-fluorescence images of FAD solutions with different concentrations. (a)–(e) Excited by 3-W LEDs at 375, 395, 405, 410, and 420 nm, respectively. The concentrations of FAD in solutions 1, 2, 3, and 4 are 0, 0.2, 1, and 2 g/L, respectively.

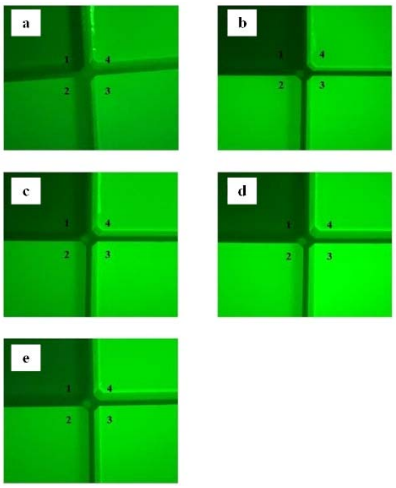

Fig. 25. Auto-fluorescence images of FAD solutions with different concentrations. (a)–(e) Excited by 5-W LEDs at 375, 395, 405, 410, and 420 nm, respectively. The concentrations of FAD in solutions 1, 2, 3, and 4 are 0, 0.2, 1, and 2 g/L, respectively.

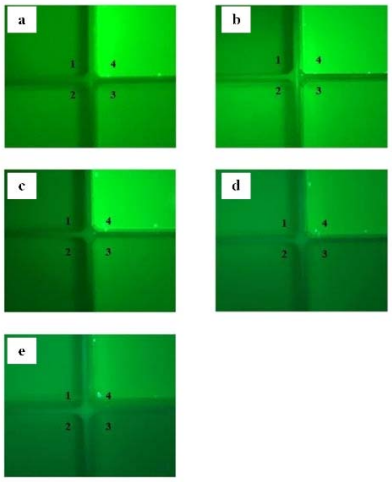

Fig. 26. Auto-fluorescence images of NADH solutions with different concentrations. (a)–(e) Excited by 3-W LEDs at 375, 395, 405, 410, and 420 nm, respectively. The concentrations of NADH in solutions 1, 2, 3, and 4 are 0, 0.8, 4, and 45 g/L, respectively.

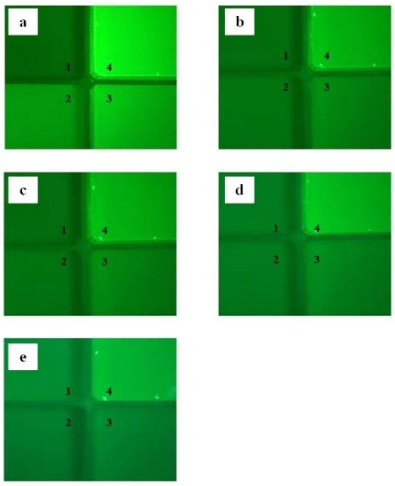

Fig. 27. Auto-fluorescence images of NADH solutions with different concentrations. (a)–(e) Excited by 5-W LEDs at 375, 395, 405, 410, and 420 nm, respectively. The concentrations of NADH in solutions 1, 2, 3, and 4 are 0, 0.8, 4, and 45 g/L, respectively.

selecting the UV-LED with specify wavelength and observing the characteristics of sublingual gland cysts.

C. Auto-Fluorescence Detection Using FAD and NADH Solutions

As mentioned previously, FAD and NADH are essential components of the two respiratory chains of the human body, therefore, both coenzymes are closely related to cell life activities. In cancerous or precancerous tissues, cells will proliferate in large numbers, and at the same time, with very vigorous glycolysis, the concentration of FAD and NADH will continue to increase. Several studies have shown that the concentrations of FAD and NADH in normal tissues and cancerous tissues are different [39], [40]. Therefore, this work verifies the applicability of auto-fluorescence detection equipment by configuring different FAD and NADH solution concentrations.

The auto-fluorescence detection results of the FAD solution are shown in Figs. 24 and 25. It can be easily seen in Fig. 16 that the fluorescence intensity of FAD increases obviously with the concentration rising. This is because the FAD emits significant auto-fluorescence under the excitation of detection equipment, demonstrating the effective detectability of the proposed method. Moreover, the contrast between different concentrations of FAD solution also varies slightly with the change of wavelengths of excitation LED. Additionally, a relatively good contrast can be obtained when using an LED with a wavelength of 405 nm. The same findings can also be obtained when using higher-power LEDs (see Fig. 25).

Meanwhile, the auto-fluorescence detection results of NADH are shown in Figs. 26 and 27. Similarly, with the

phenomenon of FAD, the fluorescence intensity of NADH also gets enhanced as the concentration increases. This illustrates that NADH also has effective auto-fluorescence when using the detection equipment. Figs. 26 and 27 show that the relatively good contrast of NADH can be obtained when using the LEDs with wavelengths of 375 and 405 nm.

V. Conclusion

To promote and popularize auto-fluorescence detection technology in the screening of oral cancer and the detection of precancerous lesions, an efficient and fast auto-fluorescence detection apparatus was designed, and the prototype was built. The proposed equipment with multiple wavelength LEDs can effectively protect the light source and prolong the device's lifetime. The capability of auto-fluorescence detection was verified from the results where detection of FAD and NADH solutions for herpes simplex and sublingual cysts was performed. In the detection process for oral diseases and coenzyme solutions, the use of excitation light of different wavelengths would affect the contrast of the fluorescence absence phenomenon, thereby improving the oral examination results.

References

[1] S. Scott, M. McGurk, and E. Grunfeld, "Patient delay for potentially malignant oral symptoms," *Eur. J. Oral Sci.*, vol. 116, no. 2, pp. 141–147, Apr. 2008.

[2] N. L. Rhodus, A. R. Kerr, and K. Patel, "Oral cancer: Leukoplakia, premalignancy, and squamous cell carcinoma," *Dental Clinics North Amer.*, vol. 58, no. 2, pp. 315–340, 2014.

[3] S. Warnakulasuriya, "Causes of oral cancer—An appraisal of controversies," *Brit. Dental J.*, vol. 207, no. 10, pp. 471–475, Nov. 2009.

[4] C. L. Vecchia, A. Tavani, S. Franceschi, F. Levi, G. Corrao, and E. Negri, "Epidemiology and prevention of oral cancer," *Oral Oncol.*, vol. 33, no. 5, pp. 302–312, Sep. 1997.

[5] S. Petti, "Lifestyle risk factors for oral cancer," *Oral Oncol.*, vol. 45, nos. 4–5, pp. 340–350, 2009.

[6] G. R. Ogden, "Alcohol and oral cancer," *Int. J. Oral Maxillofacial Surg.*, vol. 38, no. 5, p. 422, May 2009.

[7] S. Warnakulasuriya, "Areca nut use following migration and its consequences," *Addiction Biol.*, vol. 7, no. 1, pp. 127–132, Jan. 2002.

[8] X. Zhang and P. A. Reichart, "A review of betel quid chewing, oral cancer and precancer in Mainland China," *Oral Oncol.*, vol. 43, no. 5, pp. 424–430, May 2007.

[9] F. Angiero, L. B. Gatta, R. Seramondi, A. Berenzi, and E. Dessy, "Frequency and role of HPV in the progression of epithelial dysplasia to oral cancer," *Anticancer Res.*, vol. 30, no. 9, pp. 3435–3440, 2010.

[10] X. Chen, E. M. Sturgis, A. K. El-Naggar, Q. Wei, and G. Li, "Combined effects of the p53 codon 72 and p73 G4C14-to-A4T14 polymorphisms on the risk of HPV16-associated oral cancer in never-smokers," *Carcinogenesis*, vol. 29, no. 11, pp. 2120–2125, Aug. 2008.

[11] N. Sharma *et al.*, "Multifractal texture analysis of salivary fern pattern for oral pre-cancers and cancer assessment," *IEEE Sensors J.*, vol. 21, no. 7, pp. 9333–9340, Apr. 2021.

[12] M. Marsden *et al.*, "Intraoperative margin assessment in oral and oropharyngeal cancer using label-free fluorescence lifetime imaging and machine learning," *IEEE Trans. Biomed. Eng.*, vol. 68, no. 3, pp. 857–868, Mar. 2021.

[13] M. W. Lingen, J. R. Kalmar, T. Karrison, and P. M. Speight, "Critical evaluation of diagnostic aids for the detection of oral cancer," *Oral Oncol.*, vol. 44, no. 1, pp. 10–22, Jan. 2008.

[14] N. L. Rhodus, A. R. Kerr, and K. Patel, "Oral cancer: Leukoplakia, premalignancy, and squamous cell carcinoma," *Dental Clinics North Amer.*, vol. 58, no. 2, pp. 315–340, 2014.

[15] C.-H. Chan, T.-T. Huang, C.-Y. Chen, C.-C. Lee, M.-Y. Chan, and P.-C. Chung, "Texture-map-based branch-collaborative network for oral cancer detection," *IEEE Trans. Biomed. Circuits Syst.*, vol. 13, no. 4, pp. 766–780, Aug. 2019.

[16] M. O. Shaikh, C.-M. Lin, D.-H. Lee, W.-F. Chiang, I.-H. Chen, and C.-H. Chuang, "Portable pen-like device with miniaturized tactile sensor for quantitative tissue palpation in oral cancer screening," *IEEE Sensors J.*, vol. 20, no. 17, pp. 9610–9617, Sep. 2020.

[17] G. Banavar *et al.*, "The salivary metatranscriptome as an accurate diagnostic indicator of oral cancer," *NPJ Genomic Med.*, vol. 6, no. 1, pp. 1–10, Dec. 2021.

[18] P. B. Sridhara *et al.*, "Oral cancer and its epidemiology, therapy and risk factors, case studies in Karnataka: A review," *Int. J. Pharmaceutical Sci. Res.*, vol. 12, no. 11, pp. 5652–5661, 2021.

[19] D.-W. Zheng *et al.*, "Biomaterial-mediated modulation of oral microbiota synergizes with PD-1 blockade in mice with oral squamous cell carcinoma," *Nature Biomed. Eng.*, vol. 6, no. 1, pp. 32–43, Jan. 2022.

[20] S. Yete and D. Saranath, "MicroRNAs in oral cancer: Biomarkers with clinical potential," *Oral Oncol.*, vol. 110, Nov. 2020, Art. no. 105002.

[21] D. V. Messadi, "Diagnostic aids for detection of oral precancerous conditions," *Int. J. Oral Sci.*, vol. 5, no. 2, pp. 59–65, Jun. 2013.

[22] M. Petruzzi *et al.*, "Evaluation of autofluorescence and toluidine blue in the differentiation of oral dysplastic and neoplastic lesions from non dysplastic and neoplastic lesions: A cross-sectional study," *J. Biomed. Opt.*, vol. 19, no. 7, Jul. 2014, Art. no. 076003.

[23] J. A. Jo *et al.*, "Endogenous fluorescence lifetime imaging (FLIM) endoscopy for early detection of oral cancer and dysplasia," in *Proc. 40th Annu. Int. Conf. IEEE Eng. Med. Biol. Soc. (EMBC)*, Jul. 2018, pp. 3009–3012.

[24] S. N. Shaiju *et al.*, "Habits with killer instincts: *In vivo* analysis on the severity of oral mucosal alterations using autofluorescence spectroscopy," *J. Biomed. Opt.*, vol. 16, no. 8, 2011, Art. no. 087006.

[25] T.-T. Huang *et al.*, "Novel quantitative analysis of autofluorescence images for oral cancer screening," *Oral Oncol.*, vol. 68, pp. 20–26, May 2017.

[26] Y. Lalla, M. A. T. Matias, and C. S. Farah, "Assessment of oral mucosal lesions with auto-fluorescence imaging and reflectance spectroscopy," *J. Amer. Dental Assoc.*, vol. 147, no. 8, pp. 1–11, 2016.

[27] N. Vigneswaran, "Auto-fluorescence guided diagnostic evaluation of suspicious oral mucosal lesions: Opportunities, limitations, and pitfalls," *Proc. SPIE*, vol. 7883, pp. 342–347, Feb. 2011.

[28] B. Valeur and M. N. Berberan-Santos, *Molecular Fluorescence: Principles and Applications*. Hoboken, NJ, USA: Wiley, 2012.

[29] B. Wardle, *Principles and Applications of Photochemistry*. Hoboken, NJ, USA: Wiley, 2009.

[30] A. Jablonski, "Efficiency of anti-Stokes fluorescence in dyes," *Nature*, vol. 131, no. 3319, pp. 839–840, Jun. 1933.

[31] P. Atkins and J. de Paula, *Physical Chemistry*. London, U.K.: Oxford Univ. Press, 2011.

[32] M. Kasha, "Characterization of electronic transitions in complex molecules," *Discuss. Faraday Soc.*, vol. 9, pp. 14–19, Jan. 1950.

[33] G. Arakeri and P. A. Brennan, "Oral submucous fibrosis: An overview of the aetiology, pathogenesis, classification, and principles of management," *Brit. J. Oral Maxillofacial Surg.*, vol. 51, no. 7, pp. 587–593, Oct. 2013.

[34] P. A. W. van den Berg, K. A. Feenstra, A. E. Mark, H. J. C. Berendsen, and A. J. W. G. Visser, "Dynamic conformations of flavin adenine dinucleotide: Simulated molecular dynamics of the flavin cofactor related to the time-resolved fluorescence characteristics," *J. Phys. Chem. B*, vol. 106, no. 34, pp. 8858–8869, Aug. 2002.

[35] B. K. Manjunath *et al.*, "Auto-fluorescence of oral tissue for optical pathology in oral malignancy," *J. Photochem. Photobiol. B, Biol.*, vol. 73, nos. 1–2, pp. 49–59, 2004.

[36] P. M. Lane *et al.*, "Simple device for the direct visualization of oral-cavity tissue fluorescence," *J. Biomed. Opt.*, vol. 11, no. 2, 2006, Art. no. 024006.

[37] A. G. Zygogianni *et al.*, "Oral squamous cell cancer: Early detection and the role of alcohol and smoking," *Head Neck Oncol.*, vol. 3, no. 1, pp. 1–12, Dec. 2011.

[38] T.-T. Huang *et al.*, "Novel quantitative analysis of autofluorescence images for oral cancer screening," *Oral Oncol.*, vol. 68, pp. 20–26, May 2017.

[39] I. Pavlova, M. Williams, A. El-Naggar, R. Richards-Kortum, and A. Gillenwater, "Understanding the biological basis of autofluorescence imaging for oral cancer detection: high-resolution fluorescence microscopy in viable tissue," *Clin. Cancer Res.*, vol. 14, no. 8, pp. 2396–2402, 2008.

[40] S. N. Shaiju *et al.*, "Habits with killer instincts: *In vivo* analysis on the severity of oral mucosal alterations using autofluorescence spectroscopy," *J. Biomed. Opt.*, vol. 16, no. 8, 2011, Art. no. 087006.

Ning Wang (Member, IEEE) was born in 1984. He received the M.S. and Ph.D. degrees in microelectronic from Xidian University, Xi'an, China, in 2009 and 2012, respectively.

From 2012, he joined the China North Industries Group Corporation General Electronics Group, Suzhou, China, as a Research and Development Engineer and a Project Leader. From 2013 to 2015, he was a Post-Doctoral Researcher with Shanghai Jiao Tong University, Shanghai, China. Since 2015, he has been a Faculty Member with the University of Shanghai for Science and Technology, Shanghai, where he is currently an Associate Professor. His current research interests include thermoelectric energy conversions and high-speed interconnect technology.

Yuan Liu was born in 1992. He received the B.S. degree in electronic and information engineering from the Nanjing Institute of Technology, Nanjing, China, in 2016, and the M.S. degree in optical engineering from the University of Shanghai for Science and Technology, Shanghai, China, in 2019.

From 2020, he joined the 214th Research Institute of China North Industries Group Corporation Ltd., Suzhou, China, as an IC Designer Engineer. He is currently a Research Assistant with the University of Shanghai for Science and Technology. His current research interests include automobile MCU chip design and vehicle communication circuits.

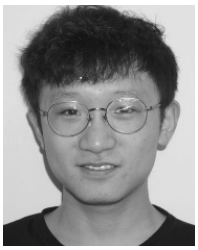

Hongwen Li was born in 1996. He received the B.S. degree in electronic science and technology from the University of Shanghai for Science and Technology, Shanghai, China, in 2018, and the M.S. degree in analytical instruments, measurement, and sensor technology from Hochschule Coburg, Coburg, Germany, in 2021.

He is currently an Electronic Engineer with Good Luck Innovative Intelligence Technology Company Ltd., Beijing, China. His current research interests include auto-fluorescence detection and thermoelectric cooling.